The dichotomy of dark matter fraction and total mass density slope of galaxies over five dex in mass

C. Tortora, L. Posti, L.V.E. Koopmans, N.R. Napolitano

Monthly Notices
of the
ROYAL ASTRONOMICAL SOCIETY

MNRAS **489,** 5483–5493 (2019)
Advance Access publication 2019 August 22

doi:10.1093/mnras/stz2320

The dichotomy of dark matter fraction and total mass density slope of galaxies over five dex in mass

C. Tortora,[1,2]★ L. Posti ,[2,3] L. V. E. Koopmans[2] and N. R. Napolitano[4,5]

[1]*INAF – Osservatorio Astrofisico di Arcetri, Largo Enrico Fermi 5, I-50125 Firenze, Italy*
[2]*Kapteyn Astronomical Institute, University of Groningen, PO Box 800, NL-9700 AV Groningen, the Netherlands*
[3]*Observatoire astronomique de Strasbourg, Université de Strasbourg, CNRS UMR 7550, 11 rue de l'Université, F-67000 Strasbourg, France*
[4]*School of Physics and Astronomy, Sun Yat-sen University Zhuhai Campus, 2 Daxue Road, Tangjia, Zhuhai, Guangdong 519082, P.R. China*
[5]*INAF – Osservatorio Astronomico di Capodimonte, Salita Moiariello, 16, I-80131 Napoli, Italy*

Accepted 2019 August 7. Received 2019 July 8; in original form 2019 February 26

ABSTRACT

We analyse the mass density distribution in the centres of galaxies across five orders of magnitude in mass range. Using high-quality spiral galaxy rotation curves and infrared photometry from SPARC, we conduct a systematic study of their central dark matter (DM) fraction ($f_{\rm DM}$) and their mass density slope (α), within their effective radius. We show that lower mass spiral galaxies are more DM dominated and have more shallow mass density slopes when compared with more massive galaxies, which have density profiles closer to isothermal. Low-mass ($M_* \lesssim 10^{10}\,{\rm M}_\odot$) gas-rich spirals span a wide range of $f_{\rm DM}$ values, but systematically lower than in gas-poor systems of similar mass. With increasing galaxy mass, the values of $f_{\rm DM}$ decrease and the density profiles steepen. In the most massive late-type gas-poor galaxies, a possible flattening of these trends is observed. When comparing these results to massive ($M_* \gtrsim 10^{10}\,{\rm M}_\odot$) elliptical galaxies from SPIDER and to dwarf ellipticals (dEs) from SMACKED, these trends result to be inverted. Hence, the values of both $f_{\rm DM}$ and α, as a function of M_*, exhibit a U-shape trend. At a fixed stellar mass, the mass density profiles in dEs are steeper than in spirals. These trends can be understood by stellar feedback from a more prolonged star formation period in spirals, causing a transformation of the initial steep density cusp to a more shallow profile via differential feedback efficiency by supernovae, and by galaxy mergers or AGN feedback in higher mass galaxies.

Key words: galaxies: elliptical and lenticular, cD – galaxies: evolution – galaxies: general – galaxies: structure – galaxies: spirals.

1 INTRODUCTION

Dark matter (DM) dominates the mass density of galaxies and clusters of galaxies. Its budget amounts to ∼85 per cent of the total mass density of the universe (e.g. Abazajian et al. 2003; Adelman-McCarthy et al. 2008; Abazajian et al. 2009) and its imprint is found on cosmological scales over the entire history of the Universe (e.g. Komatsu et al. 2011). Within the standard cosmological framework, i.e. the lambda cold dark matter (ΛCDM) model, numerical simulations of (DM only) structure formation have explained the formation of virialized DM haloes from tiny initial density perturbations, constraining the shapes and the properties of DM haloes. The spherically averaged density profile, $\rho_{\rm DM}(r)$, of DM haloes, is found to be nearly independent of halo mass and universal, and is well described by a double power-law profile with $\rho_{\rm DM}(r) \propto r^{-3}$ in the outer regions and $\rho_{\rm DM}(r) \propto r^{\alpha}$, with $\alpha < 0$, in the centre (Navarro, Frenk & White 1996, hereafter NFW; Bullock et al. 2001; Macciò, Dutton & van den Bosch 2008). However, measurements of the rotation velocities of gas in DM-dominated low-mass spiral galaxies have cast some reservations on such a universality, since the circular velocity in these systems is observed to rise linearly with radius, suggesting density cores rather than cusps ($\alpha \sim 0$, e.g. de Blok 2010). The Burkert (1995) profile is the prototype of cored models and has been shown to reproduce the DM profile of late-type galaxies (LTGs; sometimes also referred to as spiral galaxies) quite well (e.g. Salucci & Burkert 2000). Instead, in early-type galaxies (ETGs; i.e. ellipticals and lenticulars), gravitational lensing, and central stellar dynamics suggest that a cuspy profile is typically preferred (Napolitano, Romanowsky & Tortora 2010; Tortora et al. 2010b; Napolitano et al. 2011; Cappellari et al. 2013; Tortora, Romanowsky & Napolitano 2013; Tortora et al. 2014a; Mukherjee et al. 2019). Whether these differences are due to some physical process that is not entirely represented in numerical simulations, or due to a failure of the CDM paradigm, is still actively debated.

★ E-mail: ctortora@arcetri.astro.it

One way to address this problem, and constrain galaxy-formation models, is to study scaling relations among their DM halo parameters and stellar quantities. There is increasing evidence that a critical stellar mass scale around $\sim 3 \times 10^{10}\,M_\odot$ ($\sim 10^{12}\,M_\odot$ in virial mass) exists, corresponding to transitions or even breaks in the trends of different scaling relations.

If this is indeed constitutes a fundamental mass scale in galaxy structure, then it is quite plausible that also physical processes responsible for galaxy evolution change when crossing this mass scale. Such a characteristic mass is observed in the trends with galaxy mass of the total *M*/*L* and star formation efficiency (when considering all galaxies, e.g. Benson et al. 2000, Marinoni & Hudson 2002, van den Bosch et al. 2007; Conroy & Wechsler 2009; Moster et al. 2010; though it appears different when considering galaxies of different types, e.g. Dutton et al. 2010; More et al. 2011; Wojtak & Mamon 2013; Posti, Fraternali & Marasco 2018), the half-light dynamical *M*/*L* (Wolf et al. 2010; Toloba et al. 2011), the central DM fraction (Cappellari et al. 2013; Tortora, La Barbera & Napolitano 2016; Lovell et al. 2018), the $\mu_e - R_e$ (Capaccioli, Caon & D'Onofrio 1992; Tully & Verheijen 1997; Kormendy et al. 2009), and the size–mass (Shen et al. 2003; Hyde & Bernardi 2009) relations, the trends in optical colour, metallicity, and stellar *M*/*L* gradients (Kuntschner et al. 2010; Spolaor et al. 2010; Tortora et al. 2010a, 2011), as well as the gradients in the dynamical *M*/*L* profiles through several R_e (Napolitano et al. 2005).

In this paper, we uniformly analyse the stellar and DM distribution in galaxies of different types, providing some of the most comprehensive constraints on galaxy formation models over five orders of magnitude in stellar mass. Studies of the DM fraction and total mass density slope in the central regions of galaxies have particularly focused in the last years on ETGs, due to the wealth of dynamical and gravitational-lensing data (e.g. Bolton et al. 2006; Cappellari et al. 2006; Bolton et al. 2008; Tortora et al. 2009, 2012, 2014a,b, 2018; Auger et al. 2010; Thomas et al. 2011; Dutton & Treu 2014; Oguri, Rusu & Falco 2014). Using similar observables, we strive at expanding this analysis to a broader range of galaxy types, investigating the mass density profile in the central regions of late-type galaxies. In particular, we concentrate on their central DM fraction and the total mass density slope, both derived within the effective radius, R_e. We apply a uniform analysis method, which we have developed in the past for ETGs and dwarf ellipticals (dEs) (Tortora et al. 2009, 2012, 2014a,b; Tortora et al. 2016, 2018).

The central DM content in massive ETGs is very well studied (e.g. Gerhard et al. 2001; Cappellari et al. 2006; Thomas et al. 2007, 2011; Tortora et al. 2009). In particular, Tortora et al. (2016) have proposed that the DM fraction with galaxy mass exhibits a U-shape trend, with large DM fractions in both the most, and least, massive galaxies (see also Lovell et al. 2018). Furthermore, gravitational lensing and central stellar dynamics suggest that the stellar and DM profiles conspire to yield a total mass density profile which is nearly isothermal in massive ETGs (e.g. Kochanek 1991; Bolton et al. 2006; Koopmans et al. 2006, 2009; Gavazzi et al. 2007; Bolton et al. 2008; Auger et al. 2009, 2010; Chae, Bernardi & Kravtsov 2014; Oguri et al. 2014), i.e. having a total mass density profile following $\rho(r) \propto r^{\alpha}$ with $\alpha \sim -2$ and a scatter of ~ 10 per cent. However, lower masses ETGs seem to show a non-universal total mass density slope as it generally steepens at lower masses (e.g. Dutton & Treu 2014; Tortora et al. 2014a). In contrast, while the amount of dark-to-luminous matter density in the centres of spirals has been extensively studied (e.g. Swaters et al. 2014; Erroz-Ferrer et al. 2016; Lelli et al. 2016c), it is not straightforward to compare these studies with those of ETGs at face value.

To homogeneously compare the DM fractions of LTG sand ETGs, we have therefore performed an analysis of LTGs H I rotation curve data which is similar to what is usually done for central velocity dispersions of ETGs. While stellar kinematics in early-type galaxies cannot break the stellar–dark matter degeneracy, except for isolated cases which rely on excellent and spatially extended dynamical data (see e.g. Napolitano et al. 2014), for local late-type galaxies with measured extended rotation curves, the mass density profile can be directly inferred, with limited modelling assumptions and degeneracies. The SPARC sample (Lelli, McGaugh & Schombert 2016a) represents the ideal data set to perform such a study, because it combines H I kinematics (which traces the circular velocity) with 3.6 μm photometry (tracing the old stellar mass distribution). We compare the results in this paper with theoretical expectations and independent observational results for ETGs and dEs, providing an homogeneous and self-consistent picture of galaxy evolution across a wide range of masses and galaxy types.

The paper is organised as follows. In Section 2, we present the galaxy data sets that we use, the DM fraction and the mass density slope derivation. The DM fraction and the mass density slope in terms of stellar mass are presented and discussed in Section 3. In Section 4, we provide a physical interpretation of the results, while our conclusions are given in Section 5. Decimal logarithms are used in the paper. If not stated otherwise, we adopt a cosmological model with $(\Omega_m, \Omega_\Lambda, h) = (0.3, 0.7, 0.75)$, where $h = H_0/100\,\mathrm{km\,s^{-1}\,Mpc^{-1}}$ (Komatsu et al. 2011).

2 DATA SAMPLES AND ANALYSIS

In this section, we describe the data samples and the analysis adopted to derive the stellar and total mass density profiles. In Section 2.1, we start with local spiral galaxies from the SPARC sample, which span a stellar mass range from $\sim 10^7$ to $\sim 10^{11}$ $M_\odot$. In Section 2.2.1, we introduce ETGs from the SPIDER sample, while their lower mass counterparts from the SMACKED sample, i.e. dEs, are presented in Section 2.2.2.

2.1 Late-type galaxies from the SPARC sample

We start from the sample of 175 galaxies from the SPARC data base (Lelli et al. 2016a for more details) with extended H I rotation curves and *Spitzer* [3.6] photometry. Although SPARC is neither a statistically complete nor a volume-limited sample, it is representative of disc galaxies in the nearby Universe. SPARC spans a wide range in morphologies (S0 to Im/BCD), stellar masses ($\sim 10^7$ to $\sim 10^{11}$ $M_\odot$), effective radii ($\sim$0.3 to $\sim$15 kpc), rotation velocities ($\sim$20 to $\sim$300 km s^{-1}), and gas content ($0.01 \lesssim M_{\mathrm{H\,I}}/L_{[3.6]}/(M_\odot/L_\odot) \lesssim 10$). Throughout, we define the effective radius as the radius encompassing half of the total [3.6] luminosity. Lelli et al. (2016a) performed a simple photometric bulge plus disc decomposition on the sample. They find that 32 out of the original 175 galaxies have a non-negligible bulge component and concentrate at very high luminosities and low gas-mass fractions. The total luminosity is converted to a total stellar mass assuming a [3.6] stellar mass-to-light ratio, Υ_*, of $0.6\,\Upsilon_\odot$.[1] Distances to

[1]Following Lelli, McGaugh & Schombert (2016b), we assume that Υ_* is almost constant in *the* [3.6] band. Although a consensus on the overall normalization has not been reached, Lelli et al. (2016b) find that a value $\gtrsim 0.5$ minimizes the scatter in the Tully–Fisher relation, consistently with what is expected in a ΛCDM cosmology. Moreover, for the disc and bulge

these galaxies are measured in various ways. The best distance measurements, however, are determined from the tip of the red giant branch, the cepheids magnitude–period relation, the supernovae light curves, and using the distance of the cluster for galaxies in the Ursa Major cluster. The typical distance errors are ∼5 to 10 per cent, but can reach uncertainties up top 30 per cent for distances derived from the Hubble flow. These latter assume $H_0 = 73\,\mathrm{km\,s^{-1}\,Mpc^{-1}}$ and are corrected for Virgo-centric infall.

Lelli et al. (2016a) have derived rotation curves from literature data, mainly based on H I data. However, for some galaxies, hybrid rotation curves, which combine H I and H α measurements, are used. In what follows, we will consider only stars and neutral hydrogen in the baryonic mass budget, neglecting molecular gas, which should be dynamically unimportant in most circumstances (e.g. Saintonge et al. 2011).

Out of the 175 galaxies in the SPARC sample, we consider only those with inclinations larger than 30°, because the rotation velocities for nearly face-on systems are highly uncertain. This selection does not introduce any bias in the sample selection since galaxies are randomly oriented on the sky. We also cut those systems for which R_e is not covered by the rotation curve out of our final sample, in order to avoid extrapolations of the inferred rotation curve and mass distribution. We are then left with 152 out of 175 galaxies.

The deprojected mass profile $M(r)$ is determined by assuming $M(r) = V^2 r/G$, where V is the intrinsic azimuthal velocity that is obtained after deprojecting the measured velocity on the sky. The possibility to use this approximation, despite galaxies are not fully spherical, is based on the following arguments:

(i) The above formula holds for an exponential disc (within 15 per cent, see Binney & Tremaine 2008, S2.6, fig. 2.17), for a flattened spheroidal distribution (within 10 per cent, see Binney & Tremaine 2008, S2.5, fig. 2.13), and is rigorously valid for the Mestel disc model.

(ii) Since observationally we have no indications on the geometry of the DM haloes of LTGs, computing the total matter distribution with the above formula is a reasonable assumption.

(iii) Considering that the SPARC galaxies have been selected to have regular kinematics and minimal levels of non-circular motion, this mass inference should hold to good accuracy. We neglect the velocity dispersion of H I, which has a typical value of $\sim 8\,\mathrm{km\,s^{-1}}$ and yields a correction of ∼10 per cent to the velocity in most of the cases.

The total mass profile is determined by linear interpolation of the data points.[2] A more complex analysis is necessary for the mass density slope, due to the discrete measurement of the rotation curves. To avoid artefacts, we interpolate the rotation curves with polynomials. We carry out a weighted fit with a fourth order polynomial of the 10 data points closest to R_e in the observed rotation curves. We have visually inspected both the rotation curves and mass profiles, to assess the quality of the fit. All rotation curves appear well fitted. We have also verified that changing the number of points that are fitted or the order of the polynomial does not qualitatively affect our conclusions.

To determine the errors on M_*, we use the formula in Lelli et al. (2016b), propagating the errors on the distances, luminosities, and stellar M/L values. For the effective radii, we adopt an average error of 0.2 dex.[3] Finally, to calculate the errors on the DM fraction and mass density slope, we create a set of 1000 Monte Carlo realizations of the velocity profile $V(r)$, assuming Gaussian errors δV (which mainly account for differences in the approaching and receding side of the H I rotation curve). We calculate the DM fraction and mass density slope for each realization. The errors are subsequently defined as the standard deviation of the resulting distributions. We find an error of 20 and 16 per cent, respectively, on the DM fraction and mass density slopes.

2.2 ETGs and dEs

To complement the LTG analysis, here we introduce two samples of early-type systems: massive ETGs and dEs.

2.2.1 *ETGs: SPIDER sample*

For massive ETGs, we use the local ($0.05 < z < 0.095$) sample of ∼4300 giant ETGs drawn from the complete SPIDER survey (see La Barbera et al. 2010 and Tortora et al. 2012 for further details about the sample selection). The SPIDER data set includes stellar masses derived from fitting stellar population synthesis (SPS) models to their optical and near-infrared photometry (Swindle et al. 2011) using a Chabrier (2001) initial mass function (IMF). It also includes galaxy structural parameters (effective radius R_e and Sérsic index n; using 2DPHOT, La Barbera et al. 2008), homogeneously derived from g through K wavebands, and the SDSS central-aperture velocity dispersions, σ_{Ap}, within a circular fibre aperture of 1.5 arcsec radius. SPIDER ETGs are defined as luminous bulge-dominated systems, featuring passive spectra in the central SDSS fibre aperture (La Barbera et al. 2010).

2.2.2 *dEs: SMACKED sample*

At masses lower than $10^{10}\,\mathrm{M_\odot}$, we use the dEs from Tortora et al. (2016). We analyse the sample of 39 dEs in the magnitude range $-19 < M_r < -16$, selected from the Virgo Cluster Catalogue (VCC; Binggeli, Sandage & Tammann 1985). Albeit incomplete in luminosity, this sample is representative of the early-type population in this magnitude range (Toloba et al. 2014). The H-band structural parameters (the major-axis effective radius, $R_{e,\,maj}$, Sérsic index, n, and axial ratio, q) are taken from Toloba et al. (2014) and Janz et al. (2014). For nine systems without a measured value of n (as they had no fit with a single Sérsic component or are not present in Janz et al. 2014), we adopted $n = 1$. The effective velocity dispersions, σ_e, computed within an ellipse of semimajor axis length $R_{e,\,maj}$ are used (Toloba et al. 2014). We obtain the stellar H-band mass-to-light (M/L) ratio, Υ_{SSP}, for each galaxy, using the best-fitting age and metallicity from Toloba et al. (2014), and the simple stellar population (SSP) models of Vazdekis et al. (2012), for a Kroupa IMF. These Υ_{SSP} values are converted to those for a Chabrier IMF

components, SPS models suggest the following values: $\Upsilon_{bulge} = 0.7$ and $\Upsilon_{disc} = 0.5$ (e.g. Schombert & McGaugh 2014). Using these results, we assume a nominal value of $\Upsilon_* = 0.6\,\Upsilon_\odot$ for the stellar M/L. We notice that the specific value of Υ_* does not affect the calculation of total mass density slopes, but it does impact stellar mass and DM fraction calculations. We will discuss the effect of this assumption on our conclusion later in the paper and demonstrate that it will be almost negligible.

[2]We have checked that using different interpolating functions (e.g. polynomial functions of a different degree) negligibly affects our results.

[3]Unfortunately, we do not have accurate estimates for the errors on the effective radius, except for the contribution from the typical errors on distances (∼5–10 per cent). However, we assume a conservative value of 0.2 dex. The exact value of this error component will not affect our conclusions.

by subtracting 0.05 dex (i.e. the difference in normalization between the Kroupa and Chabrier IMFs; Tortora et al. 2009).

2.2.3 Model assumptions and mass modelling

According to Mamon & Łokas (2005) and Tortora et al. (2009, 2012, 2016), we model the aperture velocity dispersion of individual galaxies using the spherical isotropic Jeans equations to estimate the (total) dynamical mass $M_{\rm dyn}$ (which, we will also refer to as total mass $M_{\rm tot}$, since it includes all the mass from all the components: stars, gas, and DM). In the Jeans equations, the stellar mass density and the total mass distribution need to be specified. The stellar mass density is provided by the deprojection of the Sérsic fit of the *K*-band and *H*-band galaxy images, for SPIDER and SMACKED samples, respectively. In the following, we will present the mass models adopted for the DM or total mass distribution.

(i) *Reference NFW model with a non-universal IMF.* As a reference model, we assume a two-component model, composed of an NFW profile for the DM (motivated by *N*-body simulations) and a deprojected Sérsic profile for the stellar mass with a constant stellar *M*/*L*. This model is parametrized by the virial concentration index $c_{\rm vir}$ and the (total) virial mass $M_{\rm vir}$ (Navarro et al. 1996; Navarro, Frenk & White 1997). We fix the DM halo parameters using the correlation between $M_{\rm vir}$ and $c_{\rm vir}$, from *N*-body simulations based on WMAP5 cosmology (Macciò et al. 2008), as well as the $M_{\rm vir}$–M_* correlation from abundance matching results in Moster et al. (2010), which assumes a Chabrier IMF for M_*. For each galaxy with a Chabrier stellar mass M_*, the values of $M_{\rm vir}$ and $c_{\rm vir}$ and the DM profile are fully determined. The stellar mass derived from SPS is only used to link each galaxy to the correct halo, using the correlations mentioned above. In the stellar profile the stellar *M*/*L*, $\Upsilon_*^{\rm var}$, is free to vary. These results are taken from Tortora et al. (2013) and Tortora et al. (2014a) for the SPIDER sample and from Tortora et al. (2016) for the SMACKED sample.

Alternatives to the standard NFW profile could also be considered. In particular, the NFW profile could be steeper (due to contraction by the baryonic component; Gnedin et al. 2004). For massive ETGs, Tortora et al. (2014a) have shown that this introduces a small effect in the total mass density slopes, producing a slightly shallower trend with M_* (of ~ 5 per cent in the less massive ETGs), but increases the DM fractions (Tortora et al. 2013). We have also analysed the impact of fixing the virial mass to, e.g. a unrealistic constant value of $10^{13}\,{\rm M}_\odot$, finding a slightly shallower trend with M_*. Larger changes are induced if a Burkert profile or a high-concentration NFW model are adopted. In the latter case, very shallow average mass density slopes are found ($\alpha_{\rm mw} \sim -1.6$ at $M_* \sim 3\times10^{11}\,{\rm M}_\odot$), which do not match the results from strong lensing analysis (e.g. Koopmans et al. 2009). Instead, fixing the IMF to the standard Chabrier one in massive and high-velocity dispersion galaxies is in contrast with different results pointing to a bottom-heavy IMF (e.g. Cappellari et al. 2012; Spiniello et al. 2012; Tortora et al. 2013). For dEs, a systematic analysis of different model assumptions has been made in Tortora et al. (2016). Since the NFW model provides a fairly good and homogeneous approximation of the DM distribution in ETGs and dEs, we will adopt this model assumption in the rest of the paper, except if otherwise stated.

(ii) *Alternative models with a universal IMF.* In Section 3.4, we will compare our results with simulations, which assume a universal IMF. Indeed, we also use alternative mass profiles for both the samples, which model the total mass distribution. We assume that the mass follows the light, as $M_{\rm const-M/L}(r) = \Upsilon_{\rm tot} L(r)$, where $L(r)$ is the deprojected luminosity of the Sérsic profile, $\Upsilon_{\rm tot}$ the only free parameter of the model and we set the IMF to the Chabrier one. For the sample of massive ETGs, we also explore the case of an isothermal mass profile, which is suggested by strong lensing analyses (e.g. Koopmans et al. 2009). We assume a singular isothermal sphere (SIS) with $M_{\rm SIS}(r) \propto \sigma^2_{\rm SIS} r$ and $\sigma_{\rm SIS}$ being the free parameter. More information can be found in Tortora et al. (2012) and Tortora et al. (2016), for ETGs and dEs, respectively.

After the mass model is chosen and the predicted velocity dispersion, $\sigma_{\rm Ap}{}^J(p)$ is derived from the Jeans equation, the equation $\sigma_{\rm Ap}{}^J(p) = \sigma_{\rm Ap}$ is solved with respect to the free parameter p. The parameter p is equal to $\Upsilon_*^{\rm var}$, $\Upsilon_{\rm tot}$, and $\sigma_{\rm SIS}$ for the three models discussed above. For the SPIDER galaxies, the velocity dispersions are defined within the circular aperture of the SDSS fibre. Instead, for dEs we calculate the 3D velocity dispersion from the radial Jeans equation at the circularized (geometric) effective radius, to account for the fact that $\sigma_{\rm e}$ is averaged within an elliptic aperture, while we rely on spherical models.

3 DARK MATTER FRACTION AND MASS DENSITY SLOPE

We define the 3D de-projected DM fraction within a radius r, as $f_{\rm DM}(r) = 1 - M_{\rm b}(r)/M_{\rm tot}(r)$, where $M_{\rm b}(r)$ and $M_{\rm tot}(r)$ are the baryonic (stars and gas) and total mass as a function of the de-projected radius r. The latter includes baryons and DM (Tortora et al. 2009; Auger et al. 2010). For LTGs gas provides a non-negligible contribution to the mass budget, while it is negligible in ETGs and dEs (Courteau et al. 2014; Li et al. 2017). We also define the *mass-weighted logarithmic density slope*, $\alpha_{\rm mw}$, within a given radius r (Koopmans et al. 2009; Dutton & Treu 2014; Tortora et al. 2014a) as:

$$\alpha_{\rm mw}(r) = -3 + {\rm d}\log M_{\rm tot}(r)/{\rm d}\log r. \quad (1)$$

The value $\alpha_{\rm mw} = -2$ corresponds to a total mass density following an isothermal profile. We will calculate both $f_{\rm DM}(r)$ and $\alpha_{\rm mw}(r)$ at the 2D projected effective radius, $R_{\rm e}$, and in what follows we refer to them simply as $f_{\rm DM}$ and $\alpha_{\rm mw}$ for the sake of brevity.

3.1 Dark matter and mass density slope in SPARC LTGs

Fig. 1 shows the effective radius, $R_{\rm e}$, DM fraction within $R_{\rm e}$, $f_{\rm DM}$, the mass-weighted slope at $R_{\rm e}$, $\alpha_{\rm mw}$, as a function of total stellar mass, M_*. Data points are colour coded, in the left-hand panels, according to the gas fraction within $R_{\rm e}$. This fraction is defined as the ratio of gas and total mass within $R_{\rm e}$, $f_{\rm gas} = M_{\rm gas}(R_{\rm e})/M_{\rm tot}(R_{\rm e})$. We have verified that the impact of the gas on the central regions is negligible at $M_* \gtrsim 10^{10}\,{\rm M}_\odot$ and that, averaging across the sample, $f_{\rm gas}(R_{\rm e}) \sim 4$ per cent (median). About 83 per cent of the galaxies have $f_{\rm gas}(R_{\rm e}) < 10$ per cent. While the gas content is accounted for in the DM calculation, the mass density slope is calculated from the total mass profile.[4]

The effective radius in spiral galaxies is positively correlated with stellar mass (Courteau et al. 2007; Mosleh, Williams & Franx 2013; Lange et al. 2015; Roy et al. 2018), similarly to ETGs. The lowest mass spirals, which are also systematically gas-richer and have later morphological Hubble types, have $R_{\rm e} \sim 0.3$ kpc. The most

[4]However, we have verified that the impact of possible systematic uncertainties in the gas content on the average slopes is negligible.

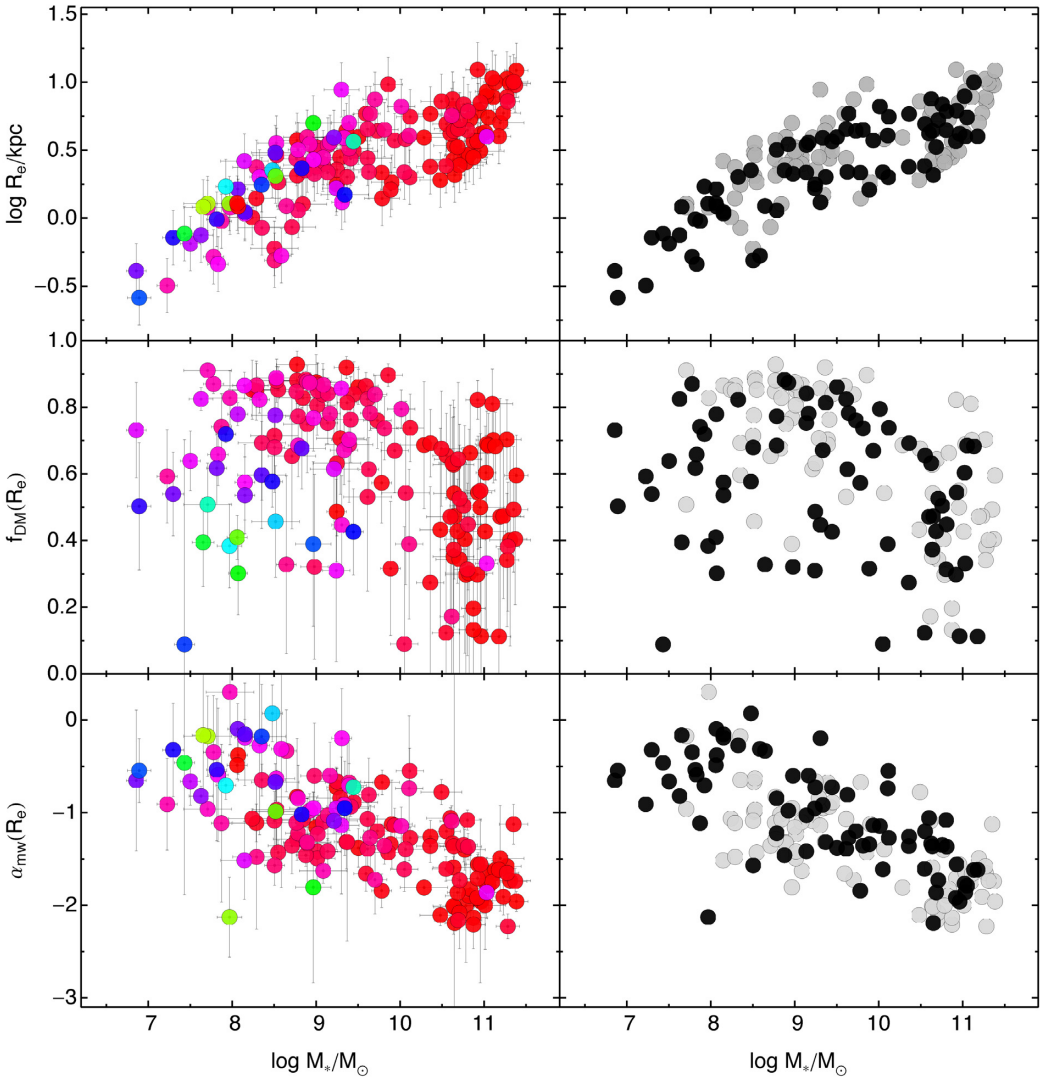

Figure 1. Effective radius R_e (top panels), DM fraction within 1 R_e f_{DM} (middle panels), and mass density slope α_{mw} (bottom panels) are plotted as a function of stellar mass, M_*, for the SPARC sample. Error bars for R_e are fixed to 0.2 dex, the errors for the other quantities are determined as described in the main text. *Left.* The points are colour coded according to the gas fraction within R_e, $f_{gas} = M_{gas}(R_e)/M_{tot}(R_e)$ (gas decreases from green, passing through blue, till to the gas poorest in red), a coloured bar is added on the top of the figure. We omit the dependence on the galaxy type, since it is providing similar changes of f_{gas}. *Right.* With black (grey) symbols we show the galaxies with more (less) accurate distance measurements (Lelli et al. 2016a).

massive spirals, typically classified as S0/Sa have $R_e \sim 10$ kpc, values similar to the sizes of massive ellipticals (see Section 3.3). For masses $\gtrsim 10^{11}$ M$_\odot$ the R_e–M_* trend is dominated by gas poorer LTGs and is steeper. This trend resembles the steep R_e–M_* correlation found in massive ETGs, with the only caveat that the SPARC sample lacks galaxies at $M_* \sim 10^{10}$ M$_\odot$, which is precisely the transition region where the trend appears to steepen. Overall, the R_e–M_* correlation is statistically significant at more than 99 per cent confidence level. We fit the relation $R_e \propto {M_*}^\gamma$ and find a slope value of $\gamma = 0.23 \pm 0.02$.

The main results are shown in the middle and bottom panels of Fig. 1. We first show the central DM fraction within one effective radius, f_{DM}, as a function of stellar mass. Spirals less massive than $\sim 10^{10}$ M$_\odot$ are more DM dominated than the most massive galaxies. We fit the relation $f_{DM} \propto {M_*}^\gamma$, finding $\gamma = -0.056 \pm 0.012$, the correlation is mild but significant at >99 per cent. Among the galaxies with $M_* \lesssim 10^{10}$ M$_\odot$, the gas-poorest ones (with $f_{gas} < 5$ per cent) have the largest DM fractions, i.e. on average $0.81^{+0.07}_{-0.18}$, where median and 16–84th quantiles of the sample distribution are quoted. Instead, the gas richer systems with $f_{gas} \geq 5$ per cent have lower f_{DM} values and a wider distribution, with a median of $0.65^{+0.21}_{-0.24}$. The most massive spirals, with $M_* \sim 10^{11}$ M$_\odot$, have DM fractions distributed in the whole range 0.1–0.8, with a median of $0.48^{+0.21}_{-0.14}$ if we only consider the galaxies with $M_* > 10^{11}$ M$_\odot$. Finally, in the bottom panel, we plot the mass density slope α_{mw} and find that it is inversely correlated with stellar mass, i.e. it is more negative at larger masses. Similarly to the previous correlations, this is also significant at more than 99 per cent and the best-fitting slope of a linear relation of the type $\alpha_{mw} = A + \gamma \log M_*$ is found to be $\gamma = -0.35 \pm 0.03$. This means that the total mass profile of spiral galaxies is getting steeper and steeper with mass. A similar regularity was already noticed by Lelli, Fraternali & Verheijen (2013), who find a tight correlation between the circular-velocity gradient in the innermost regions of galaxies and their central surface brightness. The lowest mass and gas-richest systems with $M_* \sim 10^7$ M$_\odot$ have the shallowest central slopes (i.e. $\alpha_{mw} \sim -0.5$ on average). Instead, the most massive

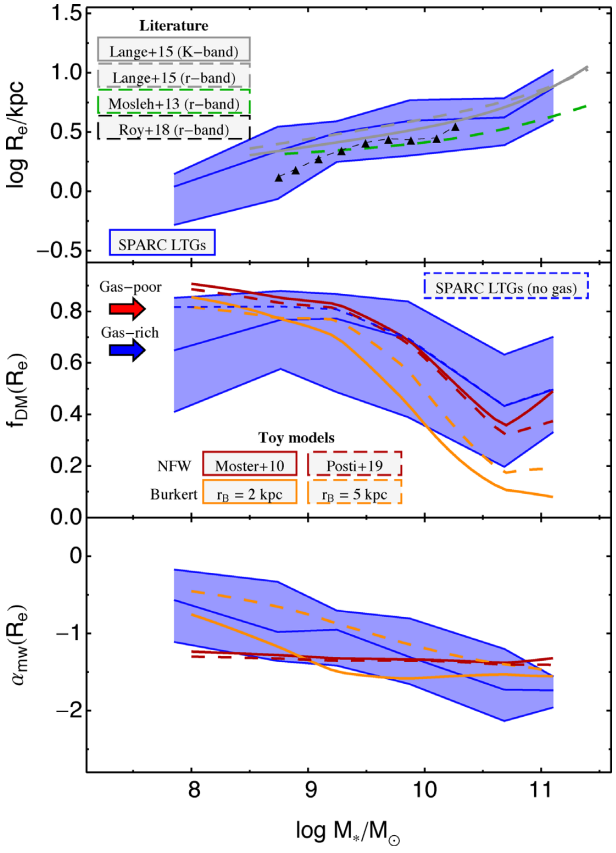

Figure 2. Effective radius, R_e, DM fraction within 1 R_e, f_{DM}, and mass density slope α_{mw} as a function of stellar mass, M_*, for the SPARC sample. Blue lines and shaded regions represent the median and 16–84th percentiles in mass bins for SPARC sample. In the top panel the R_e–M_* relation is compared with some literature (see legend, see Roy et al. 2018 for a detailed description of the plotted results from the literature). In the middle and bottom panels, red (orange) lines are the expectations from the NFW (Burkert) + baryons toy models, listed in the legend. In the middle panel, the median value of f_{DM} for gas-rich and gas-poor low-mass galaxies are also shown. See the text for more details.

(gas-poor) spirals have steeper slopes, approaching the isothermal value at the largest masses.[5]

Instead, in the right-hand panels of Fig. 1 we analyse a possible source of systematics which can come from the sample selection. In black, we plot the 73 galaxies with the best distance measurements, and we show in grey the 79 galaxies with the less accurate Hubble flow distances. We notice that the scatter and the average trends are not considerably affected by larger errors on distances. For this reason, we proceed with the whole sample of 152 galaxies.

In Fig. 2, the same results in Fig. 1 are shown as shaded regions, which represent the median and 16–84th percentiles in mass bins. In the top panel, the average size–mass relation is plotted, and compared with some literature data. In particular, we compare with the best-fitting relation in Mosleh et al. (2013) (late-type galaxies in table 1), Lange et al. (2015) (morphologically selected late-type galaxies in table 2), and Roy et al. (2018) (blue and disc-dominated galaxies), which measured R_e in r band. Mosleh et al. (2013) and Lange et al. (2015) use major axis effective radii, instead Roy et al. (2018) adopt circularized radii. We also plot the K band R_e from Lange et al. (2015), which is closer to our [3.6] effective radius.

3.2 Comparison to toy models

In the middle and bottom panels of Fig. 2, we compare the median f_{DM} and α_{mw} (plotted as blue lines and shaded regions) with the expectations from a set of toy models. For completeness we also show, as dashed blue line, the f_{DM}–M_* trend when the H I component is neglected. The effect is clearly important only at low masses, where the non-null H I gas mass decreases the DM content. Both f_{DM} and α_{mw} are derived directly from the observed velocities, without any assumption on the mass model, thus the comparison with specified DM distributions can be interesting and instructive. The toy models are based on our reference NFW and Burkert models, by computing the stellar mass model according to the exponential profile[6] (i.e. assuming Sérsic index $n = 1$) with a Chabrier IMF, and adopting the average size–mass relation of the SPARC galaxies shown in the top panel of the same figure. The model predictions do not take into account the gas content, assuming that the small fraction of H I gas is adsorbed in the DM component. This assumption does slightly impacts the observed f_{DM} trend at low masses (dashed versus solid blue lines in the midlle panel of Fig. 2). We make very simplistic assumptions, without pretending to determine the best combination of parameters reproducing both f_{DM} and α_{mw} trends. We embed the galaxies in NFW haloes assuming the c_{vir}–M_{vir} and M_{vir}–M_* correlations used for modelling ETGs and dEs (Section 2.2). In the Burkert model, the density and scale parameter (ρ_B and r_B, respectively) are assumed to follow the relation from Salucci & Burkert (2000).

The expectations for the NFW profile (plotted as a red line) reproduce quite well the trend of f_{DM} with mass, almost perfectly overlapping with the observed trend at $M_* \gtrsim 3 \times 10^9\,M_\odot$. At lower masses, the toy model is still in very good agreement with the observed median trend, especially when not considering the gas component (dashed blue line) and for gas-poor systems. The lower f_{DM} of gas-rich galaxies can be matched using smaller M_{vir} values than those predicted by the Moster relation, implying lower star formation efficiencies. On average, the total mass density slope predicted using the NFW toy models is fairly constant with mass across the whole mass range and not too far from where the observed α_{mw} lie, but it does not reproduce the steepening of the mass density slope with M_*. Toy-model DM slopes, α_{DM}, are on average ~ -1.2, consistent with the best-fitting models in Posti et al. (2018).

The models assuming Burkert profiles (with r_B values of 2 or 5 kpc) resemble quite well the observed f_{DM}–M_* trend. These models are in better agreement with lower mass spirals, but tend to have less DM than observed at $M_* \gtrsim 3 \times 10^9\,M_\odot$. The average normalization of the mass density slopes and the observed steepening with mass are, instead, reproduced quite well. This possibly indicates that spiral galaxies seem to statistically prefer a Burkert profile for the DM distribution, confirming some previous claims (Salucci & Burkert 2000). These toy models predict DM slopes

[5]Note that these massive LTGs are already DM-dominated at the effective radius, where the rotation curve is rather flat, which means that the total mass profile is isothermal.

[6]As already discussed before, Lelli et al. (2016a) have performed a photometric bulge + disc decomposition of these galaxies, finding that only 32 out of the original 175 galaxies have a non-null bulge component (27 out of 152 galaxies discussed here). These are very few galaxies and assuming also for them that a single Sérsic component can approximate their light distribution negligibly impacts our trends.

which, according to the total mass density slopes, are steepening with stellar mass. At fixed M_*, smaller r_B values produce steeper DM slopes. The analysis of this aspect is beyond the scope of this paper, and we will discuss these results more extensively in a future paper.

While an overall steepening of the slope is evident, a flattening and possibly an inversion of the trend seems to emerge in the most massive side, which is populated by earlier-type and gas-poor systems, resembling what is found in ETGs (Tortora et al. 2014a; see later for a direct comparison). This result is not surprising if we look at the size–mass trend shown in the top panel of Fig. 1, where the structural properties of these massive galaxies seem different from the other systems in the SPARC sample. This might appear at odds with the recent results of Posti et al. (2018), who, fitting the rotation curves of the SPARC galaxies, have found that the total stellar-to-halo mass ratio (computed at the virial radius) does not bend at high masses, but continues to increase up to the cosmic baryon fraction in the most massive LTGs (a similar trend was also found in Shankar et al. 2006). To analyse this apparent discrepancy, we have implemented the best-fitting M_{vir}–M_* relation found in Posti et al. (2018) in our NFW + baryons toy model, and we show the results in the middle and bottom panels of Fig. 2 (dashed red line). A different M_{vir}–M_* relation has a small impact on both f_{DM} and α_{mw}, with only a somewhat less pronounced inversion in the trend of DM fraction with respect to the reference model assuming a Moster et al. (2010) relation. Therefore, this comparison confirms a well-known result: the trend between the central f_{DM} and M_* is critically dependent first on the R_e–M_* relation and secondly on the global M_{vir}–M_* relation (e.g Tortora et al. 2012).

All these results are valid if the IMF is the same for all galaxies, and we do not have any indication that IMF is systematically changing within the SPARC sample. However, performing a dynamical modelling of spiral galaxies from the MANGA survey (mostly at $M_* \gtrsim 10^{10}\,M_\odot$), Li et al. (2017) have shown that these galaxies present a similar systematic variation with velocity dispersion than ETGs, but with a slightly different slope and a larger scatter. Their results may be applicable only for the most massive galaxies in our sample; we do not have information about IMF variations in dwarf LTGs. In general, the variation of the IMF can alter the trends of f_{DM} with velocity dispersion, as shown in Tortora et al. (2013) for ETGs, but it is not trivial to understand the impact in our Fig. 2, where f_{DM} and α_{mw} are plotted as a function of M_*. In any case, while the α_{mw}–M_* trend is negligibly affected, due to the change in the M_* values only, a variation in IMF more strongly impacts the f_{DM} trend. We cannot include in our analysis a systematic variation of IMF, which has not been clearly determined yet, but we can analyse how f_{DM} changes when the IMF is systematically changed, assuming the values $\Upsilon_* = 0.5$ and $0.7\,\Upsilon_\odot$. In these cases, the variation of f_{DM} with respect to the reference value is of $\sim\pm10$ per cent. However, a more detailed analysis of this aspect is beyond the scope of this paper.

3.3 Comparison with early-type galaxies

To complement our study we also include the results for massive ETGs from the SPIDER survey, which we have worked out in previous analysis (Tortora et al. 2012; Tortora et al. 2013, 2014b). To further study the low-mass regime, we have also considered the results for dEs using the SMACKED sample (Tortora et al. 2013).

In Fig. 3, we start showing the results for massive ETGs using the reference NFW profile with free IMF, introduced in Section 2.2.1. The reason why we consider these results as reference for ETGs is that we have demonstrated that the internal dynamics in ETGs can be realistically described if the IMF is not universal. Otherwise

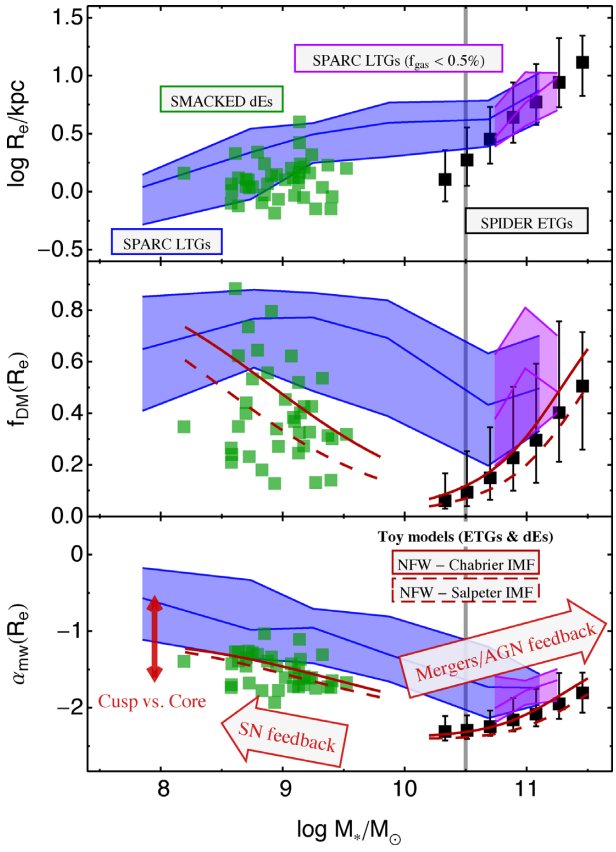

Figure 3. R_e, f_{DM}, and α_{mw} as a function of Chabrier-IMF-based stellar mass for different samples. As in Fig. 2, spirals are plotted as blue lines and shaded regions. Purple lines with shaded regions plot medians and 16–84th percentiles for LTGs with the lowest amount of gas (i.e. $f_{gas} < 0.5$ per cent). Black squares with bars are medians and 16–84th percentiles for SPIDER galaxies, assuming an NFW profile + baryons and Υ_*^{var} free. Green squares are for SMACKED dEs, assuming NFW + baryons and with Υ_*^{var} free. Red lines are toy models based on our reference NFW model and a Sérsic profile with a Chabrier (solid) and Salpeter (dashed) IMF, and adopting the size–mass relations for dEs and ETGs. The grey vertical line corresponds to the characteristic mass scale of $\sim 5 \times 10^{10}\,M_\odot$. The red arrows give information about the phenomena driving the dichotomy and their efficiency with mass. We also add a vertical arrow to point out the difference in mass density slopes among dEs and LTGs, which we relate to a cusp–core transformation in the DM distribution. See the text for more details.

we should recur to unrealistic values of c_{vir} and M_{vir} of the DM halo. The IMF is found to be 'more massive', i.e. produces a larger stellar mass, at higher velocity dispersion. However, it is pretty constant with stellar mass, pointing to a median IMF in between a Chabrier and a Salpeter IMF shape. We refer the reader to fig. 2 of Tortora et al. (2013) and fig. 1 of Tortora et al. (2014a), where these results are found and amply discussed. These results agree with a plethora of independent works using different techniques and data samples (e.g. Treu et al. 2010; Cappellari et al. 2012; Conroy & van Dokkum 2012; see Tortora et al. 2013 and Tortora et al. 2014a for a comprehensive list of references).

Thus, DM fraction within one R_e is an increasing function of stellar mass, pointing to about 50 per cent of DM in the most massive and biggest ETGs with $M_* \sim 3 \times 10^{11}\,M_\odot$ and $R_e \sim 10$ kpc. On the contrary, the lowest mass ETGs are the smallest systems with $R_e \sim 1$ kpc and with less DM (less than 10 per cent). In the bottom panel, we also show the variation of α_{mw} with mass, which points

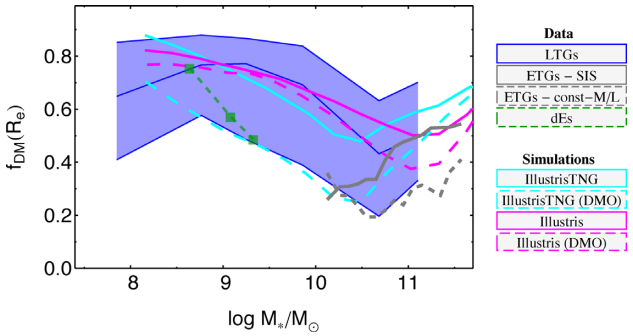

Figure 4. Comparison with cosmological simulations. We plot $f_{\rm DM}$ as a function of M_* for the different samples analysed and the outcomes from hydrodynamical simulations. Solid and dashed grey lines are medians for SPIDER ETG sample, adopting the SIS and constant-*M*/*L* models for the total mass profile, respectively, and using a Chabrier IMF. Dashed green line with squares represents the median for SMACKED dEs, assuming a constant-*M*/*L* model for the total mass profile and a Chabrier IMF. Purple and cyan lines are for simulated galaxies from Illustris and IllustrisTNG (Lovell et al. 2018). Dashed lines are created when the galaxies, simulated within the full-physics simulations (Illustris or IllustrisTNG), are placed in their corresponding DM haloes simulated within the DMO simulations.

to steeper mass density profiles at the lowest masses, approaching the isothermal law at the most massive side (see Tortora et al. 2014b for more details and results for other model assumptions). At fixed M_*, ETGs have steeper slopes than LTGs, this is driven by both the steeper stellar-mass density profiles in the former, which have systematically larger Sérsic indices, and/or steeper DM density profiles.

For consistency with ETG results, we use the same NFW with free IMF model for the dEs, and add the resulting $f_{\rm DM}$ and $\alpha_{\rm mw}$ to the plot (full green squares). The trends with stellar mass are inverted with respect to the ones found for the massive ETGs. DM fractions span a wide range of values and mass density slopes have values in the range $(-2, -1)$. The lowest mass dEs are expected to have more DM and shallower slopes.

To guide the reading of the trends, the expectations for the NFW toy models for two IMF choices are also overplotted as red lines[7] (Chabrier IMF with the solid line and Salpeter IMF with the dashed one). These toy models have $\alpha_{\rm DM} \sim -1.1$ for LTGs of all stellar masses, which is consistent with the halo fits in Posti et al. (2018), while for ETGs and dEs these are slightly shallower, but still constant with M_*, since they have smaller $R_{\rm e}$.[8] In Fig. 3, we also show the mass scale where the inversion in the trends is seen, indicating the physical processes which can lead to such different behaviours. We will discuss the physical interpretation of our results in Section 4.

3.4 Dark matter fraction from hydrodynamic simulations

Finally, in Fig. 4 we compare our $f_{\rm DM}$ with the ones from hydrodynamical simulations in Lovell et al. (2018, fig. 6).[9] Median $f_{\rm DM}$ for the Reference Illustris and IllustrisTNG simulations are shown as continuous lines. We also show the median $f_{\rm DM}$ created placing the galaxies, simulated within the full-physics simulations, in their corresponding DM haloes simulated within the DM only (DMO) simulations. These latter models neglect the effects of baryonic physics on the DM distribution. The simulation results assume a universal Chabrier IMF. They are also calculated within the deprojected half-light radius, which can be up to 1.6 times larger than the projected effective radius and the two are equivalent for galaxies with a stellar mass larger than $\sim 10^{10.5}\,{\rm M}_\odot$ (Genel et al. 2018). Therefore, the simulated $f_{\rm DM}$ could be overestimated at low masses.

To perform a more homogeneous comparison, we replace our reference results for dEs and ETGs, with the results assuming a Chabrier IMF and the two alternative models introduced in Section 2. Therefore, we adopt the SIS and constant-*M*/*L* profile for the SPIDER sample (Tortora et al. 2012), and the constant-*M*/*L* profile for the SMACKED sample (Tortora et al. 2016). The results for the reference NFW + baryons model are not shown to clutter the plot. For massive ETGs, a similar, but more gentle, variation with mass is found with respect to the reference NFW model. The SIS produces larger $f_{\rm DM}$ when compared with the reference NFW + baryons model, especially at low masses. This is expected since for this latter model (a) the IMF is 'heavier' than the Chabrier one and (b) the profile is systematically steeper than $\alpha = -2$ at low masses. On average, the steeper constant-*M*/*L* profile provides $f_{\rm DM}$ more similar to the reference model, but also an almost constant trend with M_*. For dEs, assuming the constant–*M*/*L* profile, we find larger $f_{\rm DM}$ than the reference model and a steeper trend with mass. This difference is related to the different IMF and to the higher star formation efficiency in the Moster relation, which forces $f_{\rm DM}$ to lower values when the NFW + baryon model is adopted. It is interesting to notice that the dEs and ETGs reproduce the U-shape trend independently of the mass model adopted (see Fig. 3).

Except for the TNG100 DMO simulations, the other simulations are pretty consistent with our findings for LTGs, reproducing the moderate decline in terms of M_* and the inversion of the trend at large masses. In general, the models are in better agreement with the most massive ETGs, reproducing both the trend and the normalization. This is particularly true if we consider the case of the isothermal profile in SPIDER ETGs. A good agreement is also found for the lowest mass dEs. The full-physics simulations produce large DM fractions, while the DMO simulations provide lower DM fractions, which are in better agreement with ETGs. However, a more homogeneous comparison should be made adopting the proper projected half-mass radii (or the related light-weighted values) in the simulations.

4 PHYSICAL INTERPRETATION

The results for dEs and ETGs shown in Fig. 3 point to a dichotomy of DM content and mass density slope. These results are independently confirmed by Jeans models applied to MANGA galaxies (Li et al. 2019) and results from hydrodynamic simulations (Lovell et al. 2018). Larger $f_{\rm DM}$ and shallower slopes are found in the most massive ETGs ($M_* \gtrsim 10^{11}\,{\rm M}_\odot$) and the lowest mass dEs ($M_* \sim 10^9\,{\rm M}_\odot$), and a minimum in the DM fraction and the steepest slopes are seen at the characteristic mass scale of $M_* \sim 3 \times 10^{10}\,{\rm M}_\odot$. The trends found for LTGs can, therefore, be compared with these

[7] If we consider that the NFW toy model is practically the model adopted to derive $f_{\rm DM}$ and $\alpha_{\rm mw}$ with the $\Upsilon_*^{\rm var}$ free to vary in Section 2.2, it does not surprise the very good agreement.

[8] We caution the reader that a precise comparison of the effective radii for LTGs and ETGs is not trivial, since they are determined with different approaches and in different wavebands.

[9] Unfortunately, we have not found similar results in the literature for the total mass density slope, since most of the works are focussing to small ranges of masses (typically massive ETGs), adopt variegated mass density slope definitions and probe different radial scales.

independent results. If we consider objects with a fixed mass of $\sim 10^9\,M_\odot$, then we see that LTGs are more DM dominated, within R_e, than dEs (see Fig. 1). LTGs also have shallower total density slopes than dEs of similar masses. Also, while DM fraction seems to have a more gentle variation with mass, with a plateau extending till $M_* \sim 10^{10}\,M_\odot$, the steepening of the mass density slope is found to be very similar in dEs and LTGs with $M_* \lesssim 10^{10} M_\odot$.

The U-shape behaviour of f_{DM} and α_{mw} with M_* can be understood as a result of different feedback mechanisms in these systems at different mass scales (see Fig. 3). In the lowest mass galaxies (dEs), star formation is likely inhibited by (e.g.) supernovae feedback, which is supposed to be powerful if the potential well is not too deep, as in these low-mass systems. The differences in slopes observed among dEs and LTGs of similar mass could be explained by a DM cusp–core transformation induced by such stellar feedback. Without recurring to the hypothesis of new physics about DM, within ΛCDM framework, simulations tell us that the initial cusps of DM distributions of dwarf galaxies can be transformed into cores of size approximately the 3D stellar half-light radius (i.e. of the same order of magnitude of the projected half-light radius). Multiple bursts of star formation induce a rapid expansion of the gas through supernova feedback heating (e.g. Pontzen & Governato 2012, 2014; Read, Agertz & Collins 2016). The light profiles of dEs and LTGs of similar masses are not too dissimilar, though dEs tend to be smaller. Thus, since LTGs are systematically found to have larger α_{mw}, it is likely that it is so because the DM distribution is different from that of dEs. Star formation in dEs stopped very early on, in fact they are old and red; while LTGs of similar mass had a more prolonged star formation history, thus possibly inducing larger sizes and a transformation of the original central DM density cusp into an extended core.

Low-mass galaxies, typically high-z LTGs, are built by cold streams, and present a sustained early star formation, which is then regulated by supernova feedback, with an efficiency changing with the mass of the galaxy. Supernova feedback is supposed to be more efficient in halting star formation in the lowest mass dEs and LTGs, where the potential well is not deep. Instead, the deeper potential wells in more massive galaxies are contrasting this process (Dekel & Birnboim 2006; Cattaneo et al. 2008). Therefore galaxies become more efficient in converting gas into stars, DM fractions decrease, and the initial cuspy DM distributions are less efficiently converted in shallower profiles. If not altered by external (e.g. mergers) or internal violent agents (e.g. AGN activity), this trend seems to continue up to the highest mass LTGs ($M_* \sim 10^{11} M_\odot$), where the largest star formation efficiencies are found (Posti et al. 2018). However, mergers occurring in the most massive LTGs cannot be excluded. As expected, in our sample, galaxies with a non-zero bulge-to-total mass ratio are typically found at high masses, where both secular evolution, minor and major merging can be responsible for the presence of a bulge (e.g. Weinzirl et al. 2009).

For ETGs, which dominate the high-mass end of the galaxy mass function, the situation is, instead, completely different at the $M_* \gtrsim 3 \times 10^{10}\,M_\odot$, as additional processes, such as dry merging and AGN feedback, play a fundamental role in inhibiting gas cooling and quenching their star formation (Moster et al. 2010; Tortora et al. 2010a). In fact, the trends in the total density slope found for massive ETGs can be explained by dissipation and galaxy merging occurrence. *In situ* star formation, resulting from dissipative processes, tends to form steeper-than-isothermal profiles, while gas-poor mergers are a natural attractor towards the isothermal slope (Remus et al. 2013, 2017). Thus, in ETGs with mass $\sim 3 \times 10^{10}\,M_\odot$ gas dissipation is dominant, producing more stars in the cores, smaller effective radii and f_{DM} and steeper total mass density profiles. Such low-mass ETGs cannot be formed by the merging of LTGs of similar mass, which have larger sizes and shallower slopes (Fig. 3), since such a kind of process would increase the effective radius (Naab, Johansson & Ostriker 2009; Hilz, Naab & Ostriker 2013), make the density profile shallower (e.g. Dehnen 2005), and make the galaxies more DM dominated (Tortora et al. 2018). In the most massive ETGs, galaxy (minor) mergers are producing large R_e and f_{DM} (Tortora et al. 2018) and shallower, approximately isothermal, mass profiles (Remus et al. 2013, 2017). Hence, as for the lowest mass systems, the highest mass galaxies are found to have the lowest star-formation efficiencies, the highest DM content and shallower slopes.

The U-shape trends in f_{DM} and α_{mw} for dEs, ETGs, and LTGs add up to other well-known non-monotonic correlations for galaxies (see introduction for a list of references). We found similar differences in terms of galaxy types and mass in Tortora et al. (2010a) and Tortora et al. (2011), analysing optical colour and M/L gradients in samples of local dEs, ETGs, and LTGs. dEs and ETGs manifest a similar U-shape trend with stellar mass, with the steepest colour gradients at $M_* \sim 3 \times 10^{10}\,M_\odot$. LTGs have colour gradients that follow the same steepening with mass found for dEs, but systematically steeper.

5 CONCLUSIONS

In this paper, we have investigated the DM fraction and the total mass density slopes in the central regions of late-type galaxies from the SPARC data sample (Lelli et al. 2016a), assessing how these quantities vary with stellar mass. One of the advantages of this analysis consists in the fact that observed rotation velocities provide a direct way to calculate both DM fraction and total mass density profile. While DM fraction can depend on the assumption of a universal IMF, total mass density slopes are determined without any mass modelling assumption. We find that the DM fraction is lower at the highest masses and the mass density profile is shallower in dwarf LTGs and steeper, approaching the isothermal profile, at the massive side. We describe these quantities with an approach which is coherent with previous analyses which were mainly focused on the DM fraction and mass density profile in ETGs and dEs using Jeans equations (Tortora et al. 2012; Tortora et al. 2013, 2014a).

The trend of DM fraction and mass density slope with stellar mass has a U-shape behaviour, with largest f_{DM} in most massive ETGs ($M_* \gtrsim 10^{11}\,M_\odot$) and dEs ($M_* \sim 10^9\,M_\odot$), and a minimum at $M_* \sim 3 \times 10^{10}\,M_\odot$. At low masses, we have also added the results for LTGs, which qualitatively resemble the trends with mass found for dEs, although these latter are spanning a more limited mass range. We also find that LTGs are more DM dominated and present shallower mass density slopes than dEs. We suggest that this result can be explained by a DM cusp-core transformation, induced by stellar feedback.

All these trends mirror those of the dynamical M/L (Wolf et al. 2010; Toloba et al. 2011), and of the total star formation efficiency with respect to mass and galaxy type (Benson et al. 2000, Marinoni & Hudson 2002, van den Bosch et al. 2007; Conroy & Wechsler 2009; Dutton et al. 2010; Moster et al. 2010; More et al. 2011), as such as the trend of optical colour gradients with mass (Tortora et al. 2010a, 2011) which are the result of the interplay among different physical processes, such as SN feedback at the lowest galaxy masses, and either AGN feedback and galaxy merging in the most massive passive galaxies (Tortora et al. 2010a), or an undisturbed and prolonged star formation activity in massive,

star-forming spirals (Posti et al. 2018). While in the population of LTGs the global star formation efficiency (Posti et al. 2018) and optical colour gradients (Tortora et al. 2010a) seem to be monotonic functions of the stellar mass, at $M_* \gtrsim 3 \times 10^{10}\,M_\odot$ ETGs appear to have an opposite trend, being less star forming and having shallower colour gradients as mass increases. However, even when considering spirals only, we see that we cannot exclude a flattening of f_{DM} and α_{mw} with stellar mass, since this is mostly driven by a bimodality in the mass–size (which may be due to the structure of discs, e.g. Tully & Verheijen 1997, or to the more frequent presence of bulges in high-mass LTGs).

In the future, we plan to further investigate the properties of LTGs and their mass density slopes also in terms of the environment and redshift, discriminating among central and global properties. We plan to improve these estimates also for dEs, adding more galaxies to the sample, and for ETGs, including higher quality and radially extended data, which allows to derive results which are less dependent on mass modelling (Pulsoni et al. 2018). Simulations represent a benchmark to interpret the physics behind the observational results. Defining the DM fraction and total mass density slope in a homogeneous way for both observations and simulations is a crucial step to understand the main physical processes (Mukherjee et al. 2018). We will improve this aspect using EAGLE simulations, producing mass profiles for galaxies over the 5 dex in mass analysed in this paper and studying their evolution with cosmic time.

ACKNOWLEDGEMENTS

CT and LVEK are supported through an NWO-VICI grant (project number 639.043.308). CT also acknowledges funding from the INAF PRIN-SKA 2017 program 1.05.01.88.04. LP acknowledges financial support from a VICI grant from the Netherlands Organisation for Scientific Research (NWO) and from the *Centre National d'Etudes Spatiales* (CNES). NRN acknowledges financial support from the one hundred talent program of Sun Yat-sen University and from the European Union Horizon 2020 research and innovation programme under the Marie Skodowska-Curie grant agreement no. 721463 to the SUNDIAL ITN network.

REFERENCES

Abazajian K. et al., 2003, AJ, 126, 2081
Abazajian K. N. et al., 2009, ApJS, 182, 543
Adelman-McCarthy J. K. et al., 2008, ApJS, 175, 297
Auger M. W., Treu T., Bolton A. S., Gavazzi R., Koopmans L. V. E., Marshall P. J., Bundy K., Moustakas L. A., 2009, ApJ, 705, 1099
Auger M. W., Treu T., Bolton A. S., Gavazzi R., Koopmans L. V. E., Marshall P. J., Moustakas L. A., Burles S., 2010, ApJ, 724, 511
Benson A. J., Cole S., Frenk C. S., Baugh C. M., Lacey C. G., 2000, MNRAS, 311, 793
Binggeli B., Sandage A., Tammann G. A., 1985, AJ, 90, 1681
Binney J., Tremaine S., 2008, Galactic Dynamics, 2nd edn., Princeton University Press, NJ USA
Bolton A. S., Burles S., Koopmans L. V. E., Treu T., Moustakas L. A., 2006, ApJ, 638, 703
Bolton A. S., Burles S., Koopmans L. V. E., Treu T., Gavazzi R., Moustakas L. A., Wayth R., Schlegel D. J., 2008, ApJ, 682, 964
Bullock J. S., Kolatt T. S., Sigad Y., Somerville R. S., Kravtsov A. V., Klypin A. A., Primack J. R., Dekel A., 2001, MNRAS, 321, 559
Burkert A., 1995, ApJ, 447, L25
Capaccioli M., Caon N., D'Onofrio M., 1992, MNRAS, 259, 323
Cappellari M. et al., 2006, MNRAS, 366, 1126
Cappellari M. et al., 2012, Nature, 484, 485
Cappellari M. et al., 2013, MNRAS, 432, 1862
Cattaneo A., Dekel A., Faber S. M., Guiderdoni B., 2008, MNRAS, 389, 567
Chabrier G., 2001, ApJ, 554, 1274
Chae K.-H., Bernardi M., Kravtsov A. V., 2014, MNRAS, 437, 3670
Conroy C., van Dokkum P. G., 2012, ApJ, 760, 71
Conroy C., Wechsler R. H., 2009, ApJ, 696, 620
Courteau S., Dutton A. A., van den Bosch F. C., MacArthur L. A., Dekel A., McIntosh D. H., Dale D. A., 2007, ApJ, 671, 203
Courteau S. et al., 2014, Rev. Mod. Phys., 86, 47
de Blok W. J. G., 2010, Adv. Astron., 2010, 789293
Dehnen W., 2005, MNRAS, 360, 892
Dekel A., Birnboim Y., 2006, MNRAS, 368, 2
Dutton A. A., Treu T., 2014, MNRAS, 438, 3594
Dutton A. A., Conroy C., van den Bosch F. C., Prada F., More S., 2010, MNRAS, 407, 2
Erroz-Ferrer S. et al., 2016, MNRAS, 458, 1199
Gavazzi R., Treu T., Rhodes J. D., Koopmans L. V. E., Bolton A. S., Burles S., Massey R. J., Moustakas L. A., 2007, ApJ, 667, 176
Genel S. et al., 2018, MNRAS, 474, 3976
Gerhard O., Kronawitter A., Saglia R. P., Bender R., 2001, AJ, 121, 1936
Gnedin O. Y., Kravtsov A. V., Klypin A. A., Nagai D., 2004, ApJ, 616, 16
Hilz M., Naab T., Ostriker J. P., 2013, MNRAS, 429, 2924
Hyde J. B., Bernardi M., 2009, MNRAS, 394, 1978
Janz J. et al., 2014, ApJ, 786, 105
Kochanek C. S., 1991, ApJ, 373, 354
Komatsu E. et al., 2011, ApJS, 192, 18
Koopmans L. V. E., Treu T., Bolton A. S., Burles S., Moustakas L. A., 2006, ApJ, 649, 599
Koopmans L. V. E. et al., 2009, ApJ, 703, L51
Kormendy J., Fisher D. B., Cornell M. E., Bender R., 2009, ApJS, 182, 216
Kuntschner H. et al., 2010, MNRAS, 408, 97
La Barbera F., de Carvalho R. R., Kohl-Moreira J. L., Gal R. R., Soares-Santos M., Capaccioli M., Santos R., Sant'anna N., 2008, PASP, 120, 681
La Barbera F., de Carvalho R. R., de La Rosa I. G., Lopes P. A. A., Kohl-Moreira J. L., Capelato H. V., 2010, MNRAS, 408, 1313
Lange R. et al., 2015, MNRAS, 447, 2603
Lelli F., Fraternali F., Verheijen M., 2013, MNRAS, 433, L30
Lelli F., McGaugh S. S., Schombert J. M., 2016a, AJ, 152, 157
Lelli F., McGaugh S. S., Schombert J. M., 2016b, ApJ, 816, L14
Lelli F., McGaugh S. S., Schombert J. M., Pawlowski M. S., 2016c, ApJ, 827, L19
Li H. et al., 2017, ApJ, 838, 77
Li R. et al., 2019, preprint (arXiv:1903.09282)
Lovell M. R. et al., 2018, MNRAS, 481, 1950
Macciò A. V., Dutton A. A., van den Bosch F. C., 2008, MNRAS, 391, 1940
Mamon G. A., Łokas E. L., 2005, MNRAS, 362, 95
Marinoni C., Hudson M. J., 2002, ApJ, 569, 101
More S., van den Bosch F. C., Cacciato M., Skibba R., Mo H. J., Yang X., 2011, MNRAS, 410, 210
Mosleh M., Williams R. J., Franx M., 2013, ApJ, 777, 117
Moster B. P., Somerville R. S., Maulbetsch C., van den Bosch F. C., Macciò A. V., Naab T., Oser L., 2010, ApJ, 710, 903
Mukherjee S. et al., 2018, MNRAS, 479, 4108
Mukherjee S., Koopmans L. V. E., Metcalf R. B., Tortora C., Schaller M., Schaye J., Vernardos G., Bellagamba F., 2019, preprint (arXiv:1901.01095)
Naab T., Johansson P. H., Ostriker J. P., 2009, ApJ, 699, L178
Napolitano N. R. et al., 2005, MNRAS, 357, 691
Napolitano N. R., Romanowsky A. J., Tortora C., 2010, MNRAS, 405, 2351
Napolitano N. R. et al., 2011, MNRAS, 411, 2035
Napolitano N. R., Pota V., Romanowsky A. J., Forbes D. A., Brodie J. P., Foster C., 2014, MNRAS, 439, 659
Navarro J. F., Frenk C. S., White S. D. M., 1996, ApJ, 462, 563 (NFW)
Navarro J. F., Frenk C. S., White S. D. M., 1997, ApJ, 490, 493
Oguri M., Rusu C. E., Falco E. E., 2014, MNRAS, 439, 2494
Pontzen A., Governato F., 2012, MNRAS, 421, 3464
Pontzen A., Governato F., 2014, Nature, 506, 171

Posti L., Fraternali F., Marasco A., 2019, A&A, 626, 56
Pulsoni C. et al., 2018, A&A, 618, A94
Read J. I., Agertz O., Collins M. L. M., 2016, MNRAS, 459, 2573
Remus R.-S., Burkert A., Dolag K., Johansson P. H., Naab T., Oser L., Thomas J., 2013, ApJ, 766, 71
Remus R.-S., Dolag K., Naab T., Burkert A., Hirschmann M., Hoffmann T. L., Johansson P. H., 2017, MNRAS, 464, 3742
Roy N. et al., 2018, MNRAS, 480, 1057
Saintonge A. et al., 2011, MNRAS, 415, 32
Salucci P., Burkert A., 2000, ApJ, 537, L9
Schombert J., McGaugh S., 2014, Publ. Astron. Soc. Aust., 31, e036
Shankar F., Lapi A., Salucci P., De Zotti G., Danese L., 2006, ApJ, 643, 14
Shen S., Mo H. J., White S. D. M., Blanton M. R., Kauffmann G., Voges W., Brinkmann J., Csabai I., 2003, MNRAS, 343, 978
Spiniello C., Trager S. C., Koopmans L. V. E., Chen Y. P., 2012, ApJ, 753, L32
Spolaor M., Kobayashi C., Forbes D. A., Couch W. J., Hau G. K. T., 2010, MNRAS, 408, 272
Swaters R. A., Bershady M. A., Martinsson T. P. K., Westfall K. B., Andersen D. R., Verheijen M. A. W., 2014, ApJ, 797, L28
Swindle R., Gal R. R., La Barbera F., de Carvalho R. R., 2011, AJ, 142, 118
Thomas J., Saglia R. P., Bender R., Thomas D., Gebhardt K., Magorrian J., Corsini E. M., Wegner G., 2007, MNRAS, 382, 657
Thomas J. et al., 2011, MNRAS, 415, 545
Toloba E., Boselli A., Cenarro A. J., Peletier R. F., Gorgas J., Gil de Paz A., Muñoz-Mateos J. C., 2011, A&A, 526, A114
Toloba E. et al., 2014, ApJS, 215, 17
Tortora C., Napolitano N. R., Romanowsky A. J., Capaccioli M., Covone G., 2009, MNRAS, 396, 1132
Tortora C., Napolitano N. R., Cardone V. F., Capaccioli M., Jetzer P., Molinaro R., 2010a, MNRAS, 407, 144
Tortora C., Napolitano N. R., Romanowsky A. J., Jetzer P., 2010b, ApJ, 721, L1
Tortora C., Napolitano N. R., Romanowsky A. J., Jetzer P., Cardone V. F., Capaccioli M., 2011, MNRAS, 418, 1557
Tortora C., La Barbera F., Napolitano N. R., de Carvalho R. R., Romanowsky A. J., 2012, MNRAS, 425, 577
Tortora C., Romanowsky A. J., Napolitano N. R., 2013, ApJ, 765, 8
Tortora C., La Barbera F., Napolitano N. R., Romanowsky A. J., Ferreras I., de Carvalho R. R., 2014a, MNRAS, 445, 115
Tortora C., Napolitano N. R., Saglia R. P., Romanowsky A. J., Covone G., Capaccioli M., 2014b, MNRAS, 445, 162
Tortora C., La Barbera F., Napolitano N. R., 2016, MNRAS, 455, 308
Tortora C., Napolitano N. R., Roy N., Radovich M., Getman F., Koopmans L. V. E., Verdoes Kleijn G. A., Kuijken K. H., 2018, MNRAS, 473, 969
Treu T., Auger M. W., Koopmans L. V. E., Gavazzi R., Marshall P. J., Bolton A. S., 2010, ApJ, 709, 1195
Tully R. B., Verheijen M. A. W., 1997, ApJ, 484, 145
van den Bosch F. C. et al., 2007, MNRAS, 376, 841
Vazdekis A., Ricciardelli E., Cenarro A. J., Rivero-González J. G., Díaz-García L. A., Falcón-Barroso J., 2012, MNRAS, 424, 157
Weinzirl T., Jogee S., Khochfar S., Burkert A., Kormendy J., 2009, ApJ, 696, 411
Wojtak R., Mamon G. A., 2013, MNRAS, 428, 2407
Wolf J., Martinez G. D., Bullock J. S., Kaplinghat M., Geha M., Muñoz R. R., Simon J. D., Avedo F. F., 2010, MNRAS, 406, 1220

This paper has been typeset from a TEX/LATEX file prepared by the author.